# Modal analysis of spontaneous emission in a planar microcavity

H. Rigneault and S. Monneret
*Laboratoire d'Optique des Surfaces et des Couches Minces, Unité associée au CNRS, Ecole Nationale Supérieure de Physique de Marseille, Domaine Universitaire de St. Jérôme, 13397 Marseille Cedex 20, France*
(Received 9 February 1996)

A complete set of cavity modes in planar dielectric microcavities is presented which naturally includes guided modes. We show that most of these orthonormal fields can be derived from a coherent superposition of plane waves incoming on the stack from the air and from the substrate. Spontaneous emission of a dipole located inside the microcavity is analyzed, in terms of cavity modes. Derivation of the radiation pattern in the air and in the substrate is presented. The power emitted into the guided modes is also determined. Finally, a numerical analysis of the radiative properties of an erbium atom located in a Fabry-Pérot multilayer dielectric microcavity is investigated. We show that a large amount of light is emitted into the guided modes of the structure, in spite of the Fabry-Pérot resonance, which increases the spontaneous emission rate in a normal direction. [S1050-2947(96)03908-X]

PACS number(s): 42.50.−p, 42.50.Lc, 42.55.Sa

## I. INTRODUCTION

It is now well known that spontaneous emission is not an immutable property but can be altered by modifications of the electromagnetic boundaries conditions surrounding the atom [1,2]. Optical microcavities hold technological promise for constructing efficient devices such as microlasers. The desired effects depend on the degree to which spontaneous emission may be altered by the presence of the cavity. However it has been an open question whether the cavity has to confine the waves in all three dimensions, or if a much simpler planar structure can suffice.

Spontaneous emission in a planar microcavity can be described in both frameworks of classical electromagnetism or quantum electrodynamics. The classical approach [3–6] explains the changes in the spontaneous emission in classical terms of a self-driven dipole due to the radiation reaction of the reflected field at the location of the dipole. The use of a quantum-mechanical argument [7–15] leads us to describe spontaneous emission as an emission stimulated by vacuum field fluctuations. The vacuum fluctuation and the classical radiation reaction have been shown to be the two equal contributions to the spontaneous emission process [16].

The work presented in this paper uses an orthonormal set of cavity modal fields. The conventional way of obtaining those modal fields inside a microcavity is to surround it with a large perfect cavity and to solve the eigenmode problem in the larger cavity [17]. As the dimension of the larger cavity tends to infinity, the model will approach that of a microcavity surrounded by infinitely thick material.

In case of a planar multilayer infinite microcavity, the geometry of the system does not lend itself easily to such a description. Furthermore, the construction and the normalization of the modal fields inside the larger cavity is usually a difficult and time consuming numerical problem, especially for complicated multilayer structures. One has to face two difficulties, which are

(a) the spectral continuity of modes, which present nonvanishing fields far away from the cavity (the radiation modes), and

(b) the modal field normalization problem, which is usually solved by calculating the normalizing integration [18].

Nevertheless it is possible to avoid these problems in planar dielectric structures by using a plane-wave description of the vacuum field fluctuations [9]. In this framework, each plane-wave incident from a semi-infinite uniform dielectric medium outside the microcavity is associated with a vacuum field. One can calculate the vacuum local electric field at any location inside the cavity by a classical field-transfer matrix method [19]. As mentioned above, the spontaneous emission of an atom, viewed as stimulated by the vacuum field at its location, can therefore be calculated. Thus, for every direction, one can determine whether the cavity enhances or decreases the spontaneous emission. This method has been used with success to describe radiation and lifetime properties of GaAs quantum wells in microcavities [9,20]. Nevertheless since it uses running waves in the media outside the microcavity, this method is unable to take into account guided modes, which are not coupled to traveling waves in the surrounding media.

The amount of power emitted by the atom in these guided modes might not be negligible since those modes are resonant in the stack. Furthermore, a multilayer stack can easily support several guided modes for each polarization state.

Spontaneous emission in the guided modes can be taken into account by using a complete orthogonal set of modes, which have been introduced in integrated optics for propagation problems [21,22]. This set includes a continuous spectrum, which is composed of the radiation modes, and a discrete spectrum, which is composed of the guided modes. Furthermore, the normalization, the orthogonalization, and the sampling of the continuous spectrum avoid all the numerical problems associated with the traditional method mentioned above. Those radiation modes have a plane-wave representation and can be connected to the plane-wave vacuum field description of [9].

We have outlined a quantum-mechanical analysis of the field and the emitter to predict accurately spontaneous emission rates in microcavities. A classical description can give a qualitative understanding of most of the phenomena, as well

 

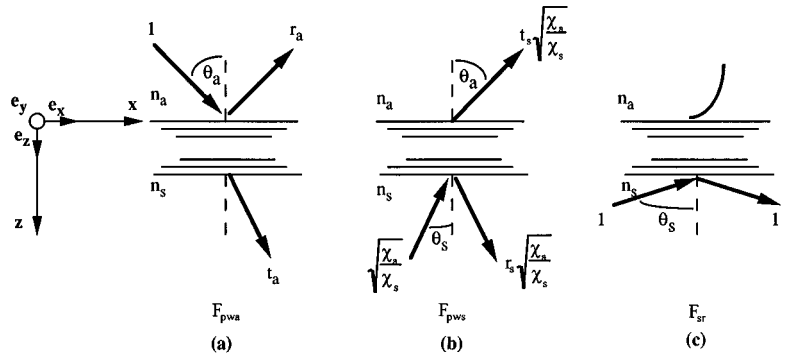


FIG. 1. Schematic view of the structure and normalized total fields resulting from plane waves incoming on the stack from the air (a), or from the substrate (b) and (c).

as quantitative predictions in comparing various structures. We choose such a classical description throughout this paper. Our work is devoted to present a modal analysis (including guided modes) to calculate spontaneous emission of an atom, considered as a dipole, and located in a planar dielectric stack.

In Sec. II, we present a plane-wave field orthonormalization in multilayer dielectric structures. A simple set of orthogonal fields is derived, which are fields resulting from a single plane wave incoming on the stack from the air or from the substrate. In Sec. III, we describe a complete set of orthogonal propagation modes, which includes radiation modes, evanescent modes, and guided modes. A simple orthonormalization of these fields is presented, and a straightforward connection with the plane-wave fields presented in Sec. II is given. In Sec. IV, we extend the modal fields orthonormalization to three dimensions. In Sec. V, we give a classical description of the spontaneous emission in dielectric multilayer microcavities in terms of cavity modes. We derive the power emitted by the dipole in the various propagation modal fields which leads to the radiation pattern in the air and in the guided modes. Finally in Sec. VI we use the theory previously presented to investigate numerically the radiative properties of an erbium atom located in various positions in a Fabry-Perot planar dielectric microcavity.

## II. PLANE-WAVE ORTHONORMALIZATION IN DIELECTRIC PLANAR MULTILAYER STRUCTURES

This part of the paper is principally devoted to normalizing $z$-dependent parts of fields that are generated in the structure when illuminated by an incident plane wave. Consider the stack of dielectric films schematically drawn in Fig. 1. The surrounding media (air and substrate) are labeled as subscripts $a$ and $s$. All the media are considered lossless, isotropic, and homogeneous. Interfaces are plane and parallel. The axes of a right-hand Cartesian coordinate frame have been chosen so that the interfaces between neighboring media are parallel to the $xy$ plane. The plane of the drawing is the $xz$ plane, which corresponds to the plane of incidence. The system is assumed to be infinite along the $x$ and $y$ directions. With these specifications the equations for TE (electric field $\mathbf{E}$ along $\mathbf{e}_y$) and TM (magnetic field $H$ along $\mathbf{e}_y$) polarizations are independent.

We consider harmonic waves with an $\exp(-i\omega t)$ temporal dependence, which will be omitted in the following calculations. For simplicity we will only consider here TE waves, the analysis being quite similar for TM waves. All the electric fields considered are thus along the $y$ axis, so we will use a scalar notation for these fields. Most of the electric fields appearing in this paper will have particular amplitude distributions, in the form $F(x,y,z)=E(z)\exp(i\beta x)$.

Consider a plane wave (wave-vector $\mathbf{k}_a$, electric-field amplitude $A_a$) incoming on the stack from the air under incidence $\theta_a$ [Fig. 1(a), where $A_a=1$]. The incident field has an amplitude in air given by

$$A_a \exp(i\beta x + i\chi_a z), \tag{1}$$

where $\beta=\mathbf{k}_a\cdot\mathbf{e}_x=2\pi n_a(\sin\theta_a/\lambda_0)$ is the propagation constant or the longitudinal spatial frequency, which has the same value in all media. Similarly,

$$\chi_a=\mathbf{k}_a\cdot\mathbf{e}_z=(n_a^2k_0^2-\beta^2)^{1/2}=n_ak_0\cos\theta_a \tag{2}$$

is the transverse spatial frequency in air.

Because the plane of incidence is assumed here to always be the plane $xz$, each of the parameters $\chi_a$ and $\beta$ can entirely define the wave-vector $\mathbf{k}_a$, for a given wavelength. By multiple reflections, the incident plane wave of amplitude $A_a$ in air gives rise to the total electric-field $F_{\mathrm{pw}a}$ in the structure, of amplitude $E_{\mathrm{pw}a}(z,\chi_a)\exp(i\beta x)$. Although this notation could seem to be not well adapted because of the dependence on the $\chi$ component with the considered medium of the stack, it will be necessary as soon we have to describe correctly the transverse cross powers of fields through the plane $xy$.

The normalization of the $z$-dependent part of the field $F_{\mathrm{pw}a}$ leads us to consider the following relation [21,22]:

$$\frac{\beta}{2\omega\mu_0}\int_{-\infty}^{+\infty}E_{\mathrm{pw}a}(z,\chi_a)E'_{\mathrm{pw}a}(z,\chi'_a)^*dz=P_a\delta(\chi_a-\chi'_a), \tag{3}$$

where $P_a$ is the cross power per unit surface in the $yz$ plane of the field $F_{\mathrm{pw}a}$. The asterisk indicates complex conjugation.

As reported in [23], this integration can be performed with some care to identify the $\delta$ function. It can be shown that all the finite terms, which result from the integration in the multilayer, cancel with each other. The infinite terms result only from the integration with infinite boundaries in the air and in the substrate, and are simply the cross power through the plane $yz$ of the incident plane wave. This power can be simply related to the amplitude $A_a$ of the incident plane wave by [23]:

$$\frac{\beta}{2\omega\mu_0}\int_{-\infty}^{+\infty} E_{\mathrm{pw}a}(z,\chi_a)E_{\mathrm{pw}a}'(z,\chi_a')^* dz = \pi A_a A_a'^* \left(\frac{\beta}{\omega\mu_0}\right)\delta(\chi_a-\chi_a'), \tag{4}$$

which leads to:

$$\int_{-\infty}^{+\infty} E_{\mathrm{pw}a}(z,\chi_a)E_{\mathrm{pw}a}'(z,\chi_a')^* dz = 2\pi A_a A_a'^* \delta(\chi_a-\chi_a'). \tag{5}$$

Equation (5) establishes not only the normalization of the $z$-dependent parts of the fields $F_{\mathrm{pw}a}$, but also their orthogonality (Kogelnik [24] gives a derivation of the orthogonality relations, which makes apparent their connection with power conservation and reciprocity).

A similar analysis holds if we now consider a second plane wave incoming on the stack from the substrate, with an amplitude $A_s$ [Fig. 1(b) where $A_s=(\chi_a/\chi_s)^{1/2}$]. By multiple reflections, this incident plane wave gives rise to the total electric-field $F_{\mathrm{pws}}$, of amplitude $E_{\mathrm{pws}}(z,\chi_s)\exp(i\beta x)$, and is assumed to have the same propagation constant $\beta$ as the wave previously considered [Fig. 1(a)]. We get the relation:

$$\int_{-\infty}^{+\infty} E_{\mathrm{pws}}(z,\chi_s)E_{\mathrm{pws}}'(z,\chi_s')^* dz = 2\pi A_s A_s'^* \delta(\chi_s-\chi_s'), \tag{6}$$

where $\chi_s=(n_s^2k_0^2-\beta^2)^{1/2}$ is the transverse spatial frequency in the substrate. Let us assume that both these incident plane waves of amplitudes $A_a$ and $A_s$ have opposite cross powers through the plane $xy$. This implies

$$\chi_s|A_s|^2=\chi_a|A_a|^2. \tag{7}$$

By choosing

$$|A_a|=1 \quad \text{and therefore} \quad |A_s|=(\chi_a/\chi_s)^{1/2}, \tag{8}$$

and since [23]

$$\chi_a\delta(\chi_s-\chi_s')=\chi_s\delta(\chi_a-\chi_a'), \tag{9}$$

we get orthonormalization relations for both the fields $F_{\mathrm{pw}a}$ and $F_{\mathrm{pws}}$ associated to the same propagation constant $\beta$ [see Figs. 1(a) and 1(b)]. This can be written as

$$\int_{-\infty}^{+\infty} E_{\mathrm{pw}a}(z,\chi_a)E_{\mathrm{pw}a}'(z,\chi_a')^* dz = 2\pi\delta(\chi_a-\chi_a'), \tag{10a}$$

$$\int_{-\infty}^{+\infty} E_{\mathrm{pws}}(z,\chi_s)E_{\mathrm{pws}}'(z,\chi_s')^* dz = 2\pi\frac{\chi_a}{\chi_s}\delta(\chi_s-\chi_s'), \tag{10b}$$

where both right-hand sides are equal.

This normalization is based on the constant amplitudes ($|A_a|=1$ and $|A_s|=(\chi_a/\chi_s)^{1/2}$) of the incident plane waves that give rise to the fields $F_{\mathrm{pw}a}$ and $F_{\mathrm{pws}}$. For a given propagation constant $\beta$, the cross powers per unit surface through the $yz$ plane of both these fields are identical, and the cross powers per unit surface through the $xy$ plane are opposite. Such properties of these normalized fields will be of great interest in Sec. III, when applied to modal field calculations.

By the way, we have considered only waves running both in the air and in the substrate. We have to also consider plane waves incoming from the substrate with a propagation constant greater than $\beta=2\pi n_a/\lambda_0$, i.e., waves running in the substrate and evanescent in the air [Fig. 1(c)]. Such a plane wave of amplitude $A_s$ gives rise to an electric-field $F_{sr}$ of amplitude $E_{sr}(z,\chi_s)\exp(i\beta x)$. It has been shown [23] that this field verifies Eq. (6), so its normalization can be achieved as previously seen.

Taking $|A_s|=1$, we get the following orthonormalization relation, similar to Eq. (10):

$$\int_{-\infty}^{+\infty} E_{sr}(z,\chi_s)E_{sr}'(z,\chi_s')^* dz = 2\pi\delta(\chi_s-\chi_s'). \tag{11}$$

Let us now briefly comment on how these sets of orthogonal fields can be used to study spontaneous emission from a quantum point of view.

Since the fields $F_{\mathrm{pw}a}$ result from plane waves incoming from the air with the same amplitude ($|A_a|=1$) but with different incidences, it is straightforward to associate each of these fields with a vacuum field. Because of multiple reflections in the stack, the vacuum field inside the cavity is then enhanced or decreased, compared to the outside unitary vacuum field. Spontaneous emission, viewed as stimulated by this vacuum field, is thus also enhanced or decreased. Although this picture seems quite simple and has been widely used to treat spontaneous emission problems, its complete justification requires a rigorous quantum analysis, which faces the difficult problem of the quantization into multilayer dielectric structures [17]. We will see further how to also use this simple set of orthogonal fields to classically study the spontaneous emission process.

As mentioned before, the fields $F_{\mathrm{pw}a}$, $F_{\mathrm{pws}}$, and $F_{sr}$ are composed of waves running in at least one of the media outside the microcavity. They are thus unable to take naturally into account guided waves. This leads us to now present a complete set of modes, which includes guided propagation inside the stack. This set of modal fields has been originally proposed by Marcuse [21] to solve propagation problems in planar integrated optics structures. Most of these modes will be defined from the fields $F_{\mathrm{pw}a}$, $F_{\mathrm{pws}}$, and $F_{sr}$.

## III. ORTHOGONAL MODES OF A PLANAR MULTILAYER DIELECTRIC STRUCTURE

The complete set of modes of a lossless multilayer dielectric structure includes an infinite number of radiation modes and evanescent modes, as well as a finite number of guided modes. The evanescent modes are neglected in this analysis since they do not carry power far away from the guide.

Because of their modal properties, the fields of the radiation modes must correspond to standing waves in the direction normal to the layers. They thus vary only by a phase factor when they propagate along the $x$ direction. These fields can be described by a superposition of two $z$-contrapropagative plane waves, which have the same cross powers through the $xy$ plane. These two waves are incoming towards the stack from the air and from the substrate, respec-

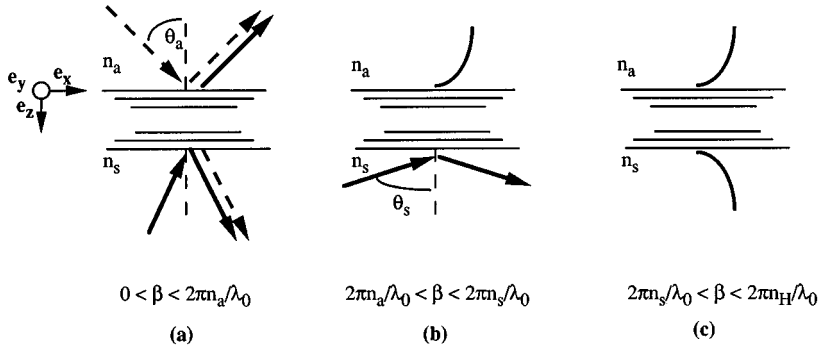


FIG. 2. Schematic views of the full radiation modes (a), substrate radiation modes (b), and guided modes (c) of planar dielectric structures.

tively, so each outgoing power is a superposition of the corresponding incoming power reflected by the stack and of the incoming power transmitted across the stack from the opposite side [Fig. 2(a)]. Two types of radiation modes are usually distinguished. The full radiation modes $(0<\beta<2\pi n_a/\lambda_0)$ radiate both in the air and in the substrate, whereas the substrate radiation modes $(2\pi n_a/\lambda_0<\beta<2\pi n_s/\lambda_0)$ radiate only in the substrate. Figures 2(a) and 2(b) give schematic views of these modes. Figure 2(c) shows a guided mode, for which $(2\pi n_s/\lambda_0<\beta<2\pi n_H/\lambda_0)$, where $n_H$ is the highest refractive index of the stack.

Using some recent works [25,26], we will now present a normalization for the radiation modes, which leads to the same relation as the one derived in Sec. II [Eqs. (10) and (11)] for the plane-wave analysis. Consider a plane-wave incident on the stack from the air with a propagation constant $\beta$, whose electric-field complex amplitude is $A_a/\sqrt{2}$ (this choice will be clarified further). Therefore the outgoing fields in the air and in the substrate have the complex amplitudes $r_aA_a/\sqrt{2}$ and $t_aA_a/\sqrt{2}$, respectively, where $r_a$ and $t_a$ are the reflection and transmission coefficients in amplitude of the stack for an incident plane wave incoming from the air [see Fig. 1(a)].

For a standing wave to be ensured, the outgoing power must equal the incoming power both in the air and in the substrate. Because we consider here a lossless structure, this can be achieved if we consider at the same time a second plane wave with complex amplitude $A_s/\sqrt{2}$ incident on the stack from the substrate, which carries the same power through the $xy$ plane. This is satisfied if we have

$$\chi_s|A_s|^2=\chi_a|A_a|^2. \tag{12}$$

Although we have clarified the intensity relationship between the two plane waves incoming on the stack from the air and from the substrate, we have not yet fixed their phase relationship [26].

Since there is no power flow perpendicular to the stack,

$$|A_a|^2=|r_aA_a+t_sA_s|^2, \tag{13}$$

where $t_s$ is the amplitude transmission coefficient of the stack for an incident plane wave incoming from the substrate [see Fig. 1(b)]. Expanding Eq. (13) leads to

$$|A_a|^2=|r_a|^2|A_a|^2+|t_s|^2|A_s|^2+2|r_a||t_s||A_a||A_s| \times\cos(\phi_{Aa}-\phi_{As}+\phi_{ra}-\phi_{ts}), \tag{14}$$

where each $\phi$ represents the phase of the complex constant designated by its subscripts. Using Eq. (12), this can be written

$$|A_a|^2=|A_a|^2(R_a+T_s)+2|r_a||t_s||A_a||A_s| \times\cos(\phi_{Aa}-\phi_{As}+\phi_{ra}-\phi_{ts}), \tag{15}$$

where $R_a=r_ar_a^*$ is the reflectivity of the stack from the air and $T_s=(\chi_a/\chi_s)t_st_s^*$ is its transmissivity from the substrate. Since we have in any case $T_s=T_a$ [19] implying $R_a+T_s=1$, this requires

$$\phi_{Aa}-\phi_{As}+\phi_{ra}-\phi_{ts}=\pm\pi/2. \tag{16}$$

Equation (16) allows us to define a particular set of radiation modes, by fixing the phase relationship between the incident plane waves of amplitudes $A_a/\sqrt{2}$ and $A_s/\sqrt{2}$. Using the fact that the phase $\phi_{ta}$ of the transmission coefficient for the wave incoming from the air equals the phase $\phi_{ts}$ of the transmission coefficient for the wave incoming from the substrate [27], Eq. (16) becomes

$$\phi_{As}=\phi_{Aa}+\phi_{ra}-\phi_{ta}\pm\pi/2. \tag{17}$$

We now choose $\phi_{Aa}=0$. Equation (17) implies that there are two possibilities to define $\phi_{As}$. Such a result is due to the fact that radiation modes having the same propagation constant $\beta$ constitute generally a bidimensional vectorial space [25,28]. So, for a given value of $\beta$, there are two full radiation modes $F_{fr-}$ and $F_{fr+}$ corresponding both to $\phi_{Aa}=0$. The electric-field $F_{fr-}$, of amplitude $E_{fr-}(z,\chi_a)\exp(i\beta x)$, results from two incident plane waves of amplitudes $A_a/\sqrt{2}$ and $A_a/\sqrt{2}\sqrt{\chi_a/\chi_s}\exp[i(\phi_{ra}-\phi_{ta}-\pi/2)]$, incoming, respectively, from the air and from the substrate. The electric-field $F_{fr+}$, of amplitude $E_{fr+}(z,\chi_a)\exp(i\beta x)$ results also from two incident plane waves, of amplitudes $A_a/\sqrt{2}$ and $A_a/\sqrt{2}\sqrt{\chi_a/\chi_s}\exp[i(\phi_{ra}-\phi_{ta}+\pi/2)]$, incoming, respectively, from the air and from the substrate. Figure 3 gives a schematic view of these two radiation modes when we choose $A_a=1$.

We will now investigate the orthonormalization relation satisfied by the radiation modes $F_{fr-}$ previously defined. The cross power through the plane $yz$ of such a given radiation mode is simply the sum of the corresponding cross powers of each of the two incident plane waves that form this mode. From Sec. II we know that this can be written as

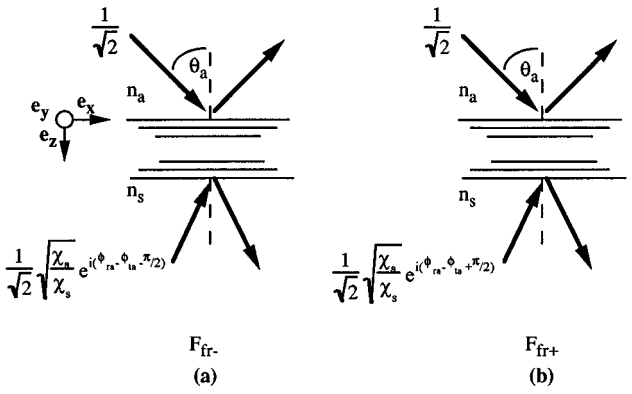


FIG. 3. Two orthogonal full radiation modes $F_{fr-}$ (a) and $F_{fr+}$ (b) associated with the same propagation constant $\beta$.

$$\frac{\beta}{2\omega\mu_0}\int_{-\infty}^{+\infty}E_{fr-}(z,\chi_a)E'_{fr-}(z,\chi'_a)^*dz = \pi\frac{A_aA'^*_a}{2}\left(\frac{\beta}{\omega\mu_0}\right)\delta(\chi_a-\chi'_a) + \pi\frac{A_sA'^*_s}{2}\left(\frac{\beta}{\omega\mu_0}\right)\delta(\chi_s-\chi'_s). \tag{18}$$

The use of Eqs. (9) and (12) leads to

$$\frac{\beta}{2\omega\mu_0}\int_{-\infty}^{+\infty}E_{fr-}(z,\chi_a)E'_{fr-}(z,\chi'_a)^*dz = \pi A_aA'^*_a\left(\frac{\beta}{\omega\mu_0}\right)\delta(\chi_a-\chi'_a). \tag{19}$$

Taking $A_a=1$, this can be simply written

$$\int_{-\infty}^{+\infty}E_{fr-}(z,\chi_a)E'_{fr-}(z,\chi'_a)^*dz=2\pi\delta(\chi_a-\chi'_a). \tag{20a}$$

The same type of derivation can be made for the radiation modes $F_{fr+}$, and gives

$$\int_{-\infty}^{+\infty}E_{fr+}(z,\chi_a)E'_{fr+}(z,\chi'_a)^*dz=2\pi\delta(\chi_a-\chi'_a). \tag{20b}$$

Consider now the substrate radiation modes, which are evanescent in the air [Fig. 2(b)]. Incident plane waves, incoming from the substrate, and having such propagation constants, are totally reflected by the stack. This leads to standing waves in the structure. Resulting electric fields are thus modal fields, and correspond to the fields denoted $F_{sr}$ in Sec. III. These substrate radiation modes are also normalized from Eq. (11). Figure 1(c) gives a schematic view of such modes.

Let us now consider the case of the guided modes [see Fig. 2(c)]. Contrary to radiation modes, which present a continuous spectrum, these guided modes only exist for discrete values of $\beta$ (namely, $\beta_g$), and present evanescent fields in the air and in the substrate. Their electric-fields $F_g$, of amplitudes $E_g(z,\chi_g)\exp(i\beta_g x)$, are of course modal since they have a zero power flow in all planes parallel to the layers. Their cross powers $P_g$ through the plane $yz$ are given by [22]

$$\frac{\beta}{2\omega\mu_0}\int_{-\infty}^{+\infty}E_g(z,\chi_g)E'_g(z,\chi'_g)^*dz=P_g\delta_{\chi_g,\chi'_g}, \tag{21}$$

where $\delta_{\chi_g,\chi'_g}$ is the Kronecker symbol.

In order to have a similar orthonormalization relation than for the full- and substrate-radiation modes, we require

$$\int_{-\infty}^{+\infty}E_g(z,\chi_g)E'_g(z,\chi'_g)^*dz=2\pi\delta_{\chi_g,\chi'_g}. \tag{22}$$

The values of the propagation constant of the guided modes are determined numerically by considering optical admittance conditions on the external interfaces of the waveguide [29]. Amplitude distributions of the guided modal fields are then derived by the use of a field-transfer matrix method [19]. Because of the finite values of their cross powers through the plane $yz$, the fields $F_g$ can thus be directly normalized from Eq. (22). This field-transfer matrix method is also well adapted to calculate the electric field that takes place in the structure when illuminated by an incident plane wave. The $z$-dependent parts $E_{\mathrm{pwa}}$, $E_{\mathrm{pws}}$, and $E_{sr}$, which have been determined in Sec. II, can thus be directly and easily determined by this method. This simplicity leads us to calculate $E_{fr+}$ and $E_{fr-}$ from $E_{\mathrm{pwa}}$, and $E_{\mathrm{pws}}$, by the use of the following relation:

$$E_{fr-}=\frac{1}{\sqrt{2}}E_{\mathrm{pwa}}+\frac{1}{\sqrt{2}}E_{\mathrm{pws}}e^{i(\phi ra-\phi ta-\pi/2)}, \tag{23a}$$

$$E_{fr+}=\frac{1}{\sqrt{2}}E_{\mathrm{pwa}}+\frac{1}{\sqrt{2}}E_{\mathrm{pws}}e^{i(\phi ra-\phi ta+\pi/2)}. \tag{23b}$$

This can be written in the matrix form

$$\begin{bmatrix}E_{fr-}\\E_{fr+}\end{bmatrix}=M\begin{bmatrix}E_{\mathrm{pwa}}\\E_{\mathrm{pws}}\end{bmatrix}, \tag{24}$$

where $M$ is the unitary transfer matrix between these two types of fields.

## IV. EXTENSION OF THE MODAL FIELDS ORTHONORMALIZATIONS TO THREE DIMENSIONS

In order to study the spontaneous emission of a dipole in a cavity, we need to extend the normalization condition to the three dimensions along the $x$, $y$, and $z$ axes. This part of the paper is thus devoted to the derivation of such a normalization. It will then be applied to the different types $F_{fr-}$, $F_{fr+}$, $F_{sr}$ and $F_g$ of modal fields of the cavity, which have been previously defined.

Consider first a plane wave of amplitude unity ($|A_a|=1$), incoming on the stack from the air with the wave-vector $\mathbf{k}_a=\beta\mathbf{e}_x+\xi\mathbf{e}_y+\chi_a\mathbf{e}_z$. From Sec. II, the total electric-field $F_{\mathrm{pwa}}$ that takes place in the stack is given by

$$\mathbf{F}_{\mathrm{pwa}}(\mathbf{r},\mathbf{k}_a)=E_{\mathrm{pwa}}(z,\chi_a)\exp(i\beta x)\exp(i\xi y)\mathbf{u}(\mathbf{k}_a), \tag{25}$$

where $\mathbf{u}(\mathbf{k}_a)$ is a TE unit electric-field vector. The extended orthonormalization relation of the field $F_{\mathrm{pw}a}$ is given by the integral

$$\int_r \mathbf{F}_{\mathrm{pw}a}(\mathbf{r},\mathbf{k}_a)\mathbf{F}_{\mathrm{pw}a}'(\mathbf{r},\mathbf{k}_a')^* d\mathbf{r} = \int_{-\infty}^{+\infty}\int_{-\infty}^{+\infty}\int_{-\infty}^{+\infty} E_{\mathrm{pw}a}(z,\chi_a)\exp(i\beta x)\exp(i\xi y) \times E_{\mathrm{pw}a}'(z,\chi_a')^*\exp(-i\beta' x) \times \exp(-i\xi' y)dx\ dy\ dz, \quad (26)$$

where $\mathbf{F}_{\mathrm{pw}a}(\mathbf{r},\mathbf{k}_a)\mathbf{F}'_{\mathrm{pw}a}(\mathbf{r},\mathbf{k}_a')^*$ represents the classical scalar product. Using Eq. (10a) and the fact that

$$\int_{-\infty}^{+\infty} \exp(i\beta x)\exp(-i\beta' x)dx = 2\pi\delta(\beta-\beta'), \quad (27)$$

we get, as in [15]

$$\int_r \mathbf{F}_{\mathrm{pw}a}(\mathbf{r},\mathbf{k}_a)\mathbf{F}_{\mathrm{pw}a}'(\mathbf{r},\mathbf{k}_a')^* d\mathbf{r} = (2\pi)^2\delta(\beta-\beta') \times \delta(\xi-\xi')\delta(\chi_a-\chi_a'), \quad (28)$$

which can be written

$$\int_r \mathbf{F}_{\mathrm{pw}a}(\mathbf{r},\mathbf{k}_a)\mathbf{F}_{\mathrm{pw}a}'(\mathbf{r},\mathbf{k}_a')^* d\mathbf{r} = (2\pi)^3\delta(\mathbf{k}_a-\mathbf{k}_a'). \quad (29)$$

Similar results are obtained for the fields $F_{\mathrm{pw}s}$ and $F_{sr}$, and Eqs. (11), (20), and (22) lead us then to define extended orthonormalization relations for all the modal fields of the cavity

$$\int_r \mathbf{F}_{fr\pm}(\mathbf{r},\mathbf{k}_a)\mathbf{F}'_{fr\pm}(\mathbf{r},\mathbf{k}_a')^* d\mathbf{r} = (2\pi)^3\delta(\mathbf{k}_a-\mathbf{k}_a'), \quad (30a)$$

$$\int_r \mathbf{F}_{sr}(\mathbf{r},\mathbf{k}_s)\mathbf{F}'_{sr}(\mathbf{r},\mathbf{k}_s')^* d\mathbf{r} = (2\pi)^3\delta(\mathbf{k}_s-\mathbf{k}_s'), \quad (30b)$$

$$\int_r \mathbf{F}_g(\mathbf{r},\mathbf{k}_g)\mathbf{F}_g'(\mathbf{r},\mathbf{k}_g')^* d\mathbf{r} = (2\pi)^3\delta(\beta-\beta')\delta(\xi-\xi')\delta_{\chi_g,\chi_g'}, \quad (30c)$$

where

$$\mathbf{F}_{fr\pm}(\mathbf{r},\mathbf{k}_a) = E_{fr\pm}(z,\chi_a)\exp(i\beta x)\exp(i\xi y)\mathbf{u}(\mathbf{k}_a), \quad (31a)$$

$$\mathbf{F}_{sr}(\mathbf{r},\mathbf{k}_s) = E_{sr}(z,\chi_s)\exp(i\beta x)\exp(i\xi y)\mathbf{u}(\mathbf{k}_s), \quad (31b)$$

$$\mathbf{F}_g(\mathbf{r},\mathbf{k}_g) = E_g(z,\chi_g)\exp(i\beta x)\exp(i\xi y)\mathbf{u}(\mathbf{k}_g). \quad (31c)$$

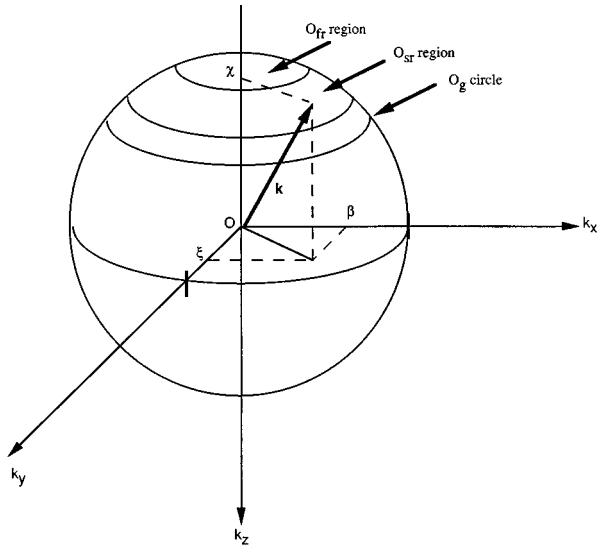


FIG. 4. Different regions in the **k** space; $O_{fr}$ (full radiation modes), $O_{sr}$ (substrate radiation modes), and $O_g$ (guided mode). We assume here only one guided mode.

## V. CLASSICAL DESCRIPTION OF THE SPONTANEOUS EMISSION IN PLANAR DIELECTRIC STRUCTURES

This part of the paper is devoted to a classical description of the spontaneous emission process in terms of cavity modes [30–32]. Such a study is based on the expansion of the total electric-field emitted by the atom on the complete set of modal fields presented in Sec. III. This leads us to take entirely into account the spontaneous emission, and to derive the emitted powers in the different modes. At this point, we will be able to compare the amounts of power emitted by the atom into the running waves, which form the radiation patterns in the air and in the substrate, and into the guided modes.

The total electric-field $\mathbf{E}(\mathbf{r},t)$ emitted by the atom, considered as a dipole, can be expanded on the propagation modal fields in the two complementary polarization states TE and TM. This can be written as

$$\mathbf{E}(\mathbf{r},t) = \sum_{\chi_g}\int_{O_g} \alpha_g(t,\mathbf{k}_g)\mathbf{F}_g(\mathbf{r},\mathbf{k}_g)d\beta\ d\xi + \int_{O_{fr}} [\alpha_{fr-}(t,\mathbf{k}_a)\mathbf{F}_{fr-}(\mathbf{r},\mathbf{k}_a) + \alpha_{fr+}(t,\mathbf{k}_a)\mathbf{F}_{fr+}(\mathbf{r},\mathbf{k}_a)]d\mathbf{k}_a + \int_{O_{sr}} \alpha_{sr}(t,\mathbf{k}_s)\mathbf{F}_{sr}(\mathbf{r},\mathbf{k}_s)d\mathbf{k}_s + (\mathrm{TM\ term}), \quad (32)$$

where each $\alpha$ contains the complete temporal dependence of its corresponding field component. $O_{fr}$, $O_{sr}$, and $O_g$ are the regions in the **k** space, which correspond, respectively, to the full radiation modes, to the substrate radiation modes, and to the guided modes. Figure 4 clarifies the definitions of these different regions in the **k** space.

The propagation of the electric field in a system containing a dipole distribution $\mathbf{p}(\mathbf{r},t)$ and a current density $\mathbf{j}(\mathbf{r},t)$ is described by the equation

$$\Delta\mathbf{E}(\mathbf{r},t)-\epsilon(z)\mu_0\frac{\partial^2\mathbf{E}}{\partial t^2}(\mathbf{r},t)=\mu_0\frac{\partial^2\mathbf{p}}{\partial t^2}(\mathbf{r},t)+\mu_0\frac{\partial\mathbf{j}}{\partial t}(\mathbf{r},t), \tag{33}$$

where we take for the dipole distribution a charge $q$, oscillating along a unit vector $\mathbf{e}$ with an amplitude $a(t)$, and located at $\mathbf{r}_0$.

$$\mathbf{p}(\mathbf{r},t)=qa(t)\delta(\mathbf{r}-\mathbf{r}_0)\mathbf{e}. \tag{34}$$

We introduce as well a dissipative volume current density $\mathbf{j}(\mathbf{r},t)$, whose amplitude is assumed to be proportional to the total electric-field $\mathbf{E}(\mathbf{r},t)$. This current will tend toward zero at the end of the derivation since we are dealing with lossless structures.

$$\mathbf{j}(\mathbf{r},t)=\epsilon(z)\Gamma\mathbf{E}(\mathbf{r},t). \tag{35}$$

As the propagation modal fields have been derived without sources, they verify the Helmholtz equation. Considering, for example, the $F_{fr}$ modes (where $F_{fr}$ stands for $F_{fr-}$ or $F_{fr+}$) we get

$$\Delta[\mathbf{F}_{fr}(\mathbf{r},\mathbf{k}_a)]+\omega_k^2\epsilon(z)\mu_0\mathbf{F}_{fr}(\mathbf{r},\mathbf{k}_a)=0 \quad \text{with} \quad \omega_k^2=\frac{k_a^2c^2}{n_a^2}. \tag{36}$$

Inserting Eq. (32) into Eq. (33) and projecting both sides of Eq. (33) on $\mathbf{F}_{fr}(\mathbf{r},\mathbf{k}_a)$, and then taking into account Eq. (36), leads to

$$\frac{\partial^2\alpha_{fr}(t,\mathbf{k}_a)}{\partial t^2}+\Gamma\frac{\partial\alpha_{fr}(t,\mathbf{k}_a)}{\partial t}+\omega_k^2\alpha_{fr}(t,\mathbf{k}_a)=-\frac{q}{(2\pi)^3\epsilon(z_0)}\frac{\partial^2a(t)}{\partial t^2}[\mathbf{e}\cdot\mathbf{F}_{fr}^*(\mathbf{r}_0,\mathbf{k}_a)], \tag{37}$$

where the last term of the right-hand side stands for the conventional scalar product between the dipole unit vector $\mathbf{e}$ and the conjugate of the modal field vector $\mathbf{F}_{fr}(\mathbf{r}_0,\mathbf{k}_a)$. Equation (37) shows that each mode behaves as a harmonic oscillator driven by an external source, whose amplitude is proportional to the dipole acceleration. Similar equations can be obtained to describe the temporal evolutions of $\alpha_{sr}(t,\mathbf{k}_s)$ and $\alpha_g(t,\mathbf{k}_g)$.

The equation describing the temporal evolution of the dipole is

$$\frac{\partial^2a(t)}{\partial t^2}+\omega_0^2a(t)=\frac{q}{m}[\mathbf{e}\cdot\mathbf{E}(\mathbf{r}_0,t)], \tag{38}$$

where $\omega_0$ is the bare dipole frequency.

We assume now a low coupling regime between the dipole and the electromagnetic field. This is the case in our multilayer stack, where the dipole is coupled to a continuum of cavity modes. In other words, we assume that the dipole perturbation due to the transverse cavity field is weak enough, so that we can neglect it in computing the total field in the cavity. We consider therefore that $[\partial^2a(t)/\partial t^2]=-\omega_0^2a(t)$ in Eq. (37), which gives

$$\alpha_{fr}(t,\mathbf{k}_a)=-\frac{qa(t)}{(2\pi)^3\epsilon(z_0)}\frac{\omega_0^2}{\omega_0^2-\omega_k^2+i\Gamma\omega_0}[\mathbf{e}\cdot\mathbf{F}_{fr}^*(\mathbf{r}_0,\mathbf{k}_a)]. \tag{39}$$

The mode expansion coefficient $\alpha_{fr}$ is proportional both to the projection of the modal field onto the dipole unit vector evaluated at the location of the dipole, and to a complex Lorentzian function. Similar results are obtained when we consider the coefficients $\alpha_{sr}(t,\mathbf{k}_s)$ and $\alpha_g(t,\mathbf{k}_g)$.

Now that we have derived the field evolution, let us come back to the temporal dipole evolution. Inserting Eq. (39) (and similar equations for $\alpha_{sr}(t,\mathbf{k}_s)$ and $\alpha_g(t,\mathbf{k}_g)$) into Eq. (38) and using Eq. (32), we obtain the evolution of the dipole

$$\frac{\partial^2a(t)}{\partial t^2}+\omega_0^2a(t)=-\frac{q^2a(t)}{m(2\pi)^3\epsilon(z_0)}\mathcal{S}\left[\frac{\omega_0^2}{\omega_0^2-\omega_k^2+i\Gamma\omega_0}\right], \tag{40}$$

where $\mathcal{S}[X(\omega_k)]$ stands for

$$\begin{aligned}\mathcal{S}[X(\omega_k)]=&\sum_{\chi_g}\int_{O_g}X(\omega_k)|\mathbf{e}\cdot\mathbf{F}_g(\mathbf{r}_0,\mathbf{k}_g)|^2d\beta\,d\xi\\&+\int_{O_{fr}}X(\omega_k)[|\mathbf{e}\cdot\mathbf{F}_{fr-}(\mathbf{r}_0,\mathbf{k}_a)|^2\\&+|\mathbf{e}\cdot\mathbf{F}_{fr+}(\mathbf{r}_0,\mathbf{k}_a)|^2]d\mathbf{k}_a+\int_{O_{sr}}X(\omega_k)\\&\times|\mathbf{e}\cdot\mathbf{F}_{sr}(\mathbf{r}_0,\mathbf{k}_s)|^2d\mathbf{k}_s+(\text{TM term}).\end{aligned} \tag{41}$$

Assuming that $a(t)=a_0\exp(-i\Omega_0t)$ with $\Omega_0=\omega_0+\delta\Omega$, we get the small complex frequency shift

$$\delta\Omega=\frac{q^2}{2m\omega_0(2\pi)^3\epsilon(z_0)}\mathcal{S}\left[\frac{\omega_0^2}{\omega_0^2-\omega_k^2+i\Gamma\omega_0}\right]. \tag{42}$$

This enables us to express explicitly the dipole damping rate $\gamma$, defined as the ratio of the total power radiated at the infinite over the dipole mechanical energy.

$$\gamma=-2\,\mathrm{Im}(\delta\Omega)=\frac{q^2}{m(2\pi)^3\epsilon(z_0)}\mathcal{S}\left[\frac{\omega_0^2\Gamma}{(\omega_0^2-\omega_k^2)^2+\Gamma^2\omega_0^2}\right], \tag{43}$$

which can be written

$$\gamma=\frac{q^2\pi}{2m(2\pi)^3\epsilon(z_0)}\mathcal{S}[\delta_\Gamma(\omega_0-\omega_k)], \tag{44}$$

where we have considered $\omega_0+\omega_k\approx2\omega_0$. The normalized Lorentz function $\delta_\Gamma(\omega_0-\omega_k)$ of width $\Gamma$ is defined by

$$\delta_\Gamma(\omega_0-\omega_k)=\frac{1}{\pi}\frac{\Gamma/2}{(\omega_0-\omega_k)^2+\Gamma^2/4}. \tag{45}$$

Multiplying (44) by the dipole mechanical energy $(1/2)ma_0^2\omega_0^2$, we get the dipole radiation power $P$ as a sum over the modal fields contributions.

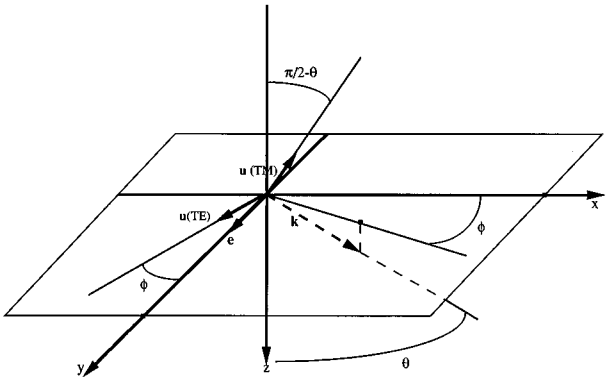


FIG. 5. Coordinate frame for the calculation of the dipole emission.

$$P=\frac{q^2a_0^2\omega_0^2\pi}{4(2\pi)^3\epsilon_0 n^2(z_0)}\,\mathcal{S}\,[\,\delta_\Gamma(\omega_0-\omega_k)]. \tag{46}$$

Let us discuss now the limiting case of a dipole radiating in an infinitely thick material of refractive index $n=n(z_0)$ considered above. In this case, only the full radiative modes $F_{fr-}(\mathbf{r},\mathbf{k})$ and $F_{fr+}(\mathbf{r},\mathbf{k})$ remain. The dipole radiation power is given by

$$P=\frac{q^2a_0^2\omega_0^2\pi}{4(2\pi)^3\epsilon_0 n^2}\int_{O_{fr}}\delta_\Gamma(\omega_0-\omega_k)[|\mathbf{e}\cdot\mathbf{F}_{fr-}(\mathbf{r}_0,\mathbf{k})|^2 + |\mathbf{e}\cdot\mathbf{F}_{fr+}(\mathbf{r}_0,\mathbf{k})|^2]d\mathbf{k}+(\text{TM term}). \tag{47}$$

It is easy to show (see Appendix A) that in the bulk material

$$|\mathbf{e}\cdot\mathbf{F}_{fr-}(\mathbf{r}_0,\mathbf{k})|^2+|\mathbf{e}\cdot\mathbf{F}_{fr+}(\mathbf{r}_0,\mathbf{k})|^2=2|\mathbf{e}\cdot\mathbf{u}(\mathbf{k})|^2, \tag{48}$$

and Eq. (47) reads

$$P=\frac{q^2a_0^2\omega_0^2\pi}{4(2\pi)^3\epsilon_0 n^2}\int_{\omega=0}^{+\infty}\frac{n^3\omega_k^2}{c^3}\,\delta_\Gamma(\omega_0-\omega_k) \times d\omega_k\int_{\theta=0}^{\pi/2}\sin\theta\int_{\phi=0}^{2\pi}2(\cos^2\phi + \sin^2\phi\,\cos^2\theta)d\theta\,d\phi, \tag{49}$$

where spherical coordinates have been used (see Fig. 5), with

$$d\mathbf{k}=\frac{n^3\omega_k^2}{c^3}\sin\theta d\theta d\phi d\omega_k\,. \tag{50}$$

The range of $\theta$ is $[0,\pi/2]$ by definition of the propagation modal fields $F_{fr-}(\mathbf{r},\mathbf{k})$ and $F_{fr+}(\mathbf{r},\mathbf{k})$ used here. The term in the integral over $\phi$ stands for the scalar product $2|\mathbf{e}\cdot\mathbf{u}|^2$, where we have placed the dipole along the $y$ axis, and considered both the contributions of the polarization states TE and TM.

It can easily be shown that

$$\int_{\theta=0}^{\pi/2}\sin\theta\int_{\phi=0}^{2\pi}2(\cos^2\phi+\sin^2\phi\,\cos^2\theta)d\theta\,d\phi=\frac{8\pi}{3} \tag{51}$$

Consider now $\Gamma=0$, corresponding to a lossless material. Since the normalized Lorentz function $\delta_\Gamma(\omega_0-\omega_k)$ tends to the Dirac distribution $\delta(\omega_0-\omega_k)$ when $\Gamma$ tends to 0, the total power radiated by the dipole is expressed by

$$P=\frac{q^2a_0^2\omega_0^4 n}{12\pi\epsilon_0 c^3}=nP_0(\omega_0), \tag{52}$$

where $P_0(\omega_0)$ is the total power radiated by a dipole in free space [33].

Let us now come back to the dipole emission in a planar lossless multilayer structure. Using spherical coordinates, Eq. (46) with $\Gamma=0$ reads

$$P=\frac{3P_0(\omega_0)}{8\pi}\left\{\frac{c}{\omega_0 n^2(z_0)}\sum_{k_g}N_{\text{eff}}^2\int_{\phi=0}^{2\pi}\left|\mathbf{e}\cdot\mathbf{F}_g(\mathbf{r}_0,\mathbf{k}_g)\right|^2 d\phi + \frac{n_a^3}{n^2(z_0)}\int_{\theta=0}^{\pi/2}\sin\theta_a\int_{\phi=0}^{2\pi}[|\mathbf{e}\cdot\mathbf{F}_{fr-}(\mathbf{r}_0,\mathbf{k}_a)|^2 + |\mathbf{e}\cdot\mathbf{F}_{fr+}(\mathbf{r}_0,\mathbf{k}_a)|^2]d\theta_a d\phi + \frac{n_s^3}{n^2(z_0)}\int_{\theta=\theta_c}^{\pi/2} \times\sin\theta_s\int_{\phi=0}^{2\pi}\left|\mathbf{e}\cdot\mathbf{F}_{sr}(\mathbf{r}_0,\mathbf{k}_s)\right|^2 d\theta_s d\phi\right\}+(\text{TM term}), \tag{53}$$

where $\theta_c=\arcsin(n_a/n_s)$ is the critical angle of total reflection for a plane wave incoming on the stack from the substrate, and where each $N_{\text{eff}}=k_g/k_0$ is one of the effective refractive indices of the guided modes. Equation (53) permits us to determine the different powers, which are emitted in each modal field. Appendix B clarifies the derivation of the first term on its right-hand side, which describes the guided mode contribution.

The dipole radiation power can also be written using the fields $F_{\text{pw}a}$ and $F_{\text{pws}}$ presented in Sec. I. Appendix A shows that

$$|\mathbf{e}\cdot\mathbf{F}_{fr-}(\mathbf{r}_0,\mathbf{k}_a)|^2+|\mathbf{e}\cdot\mathbf{F}_{fr+}(\mathbf{r}_0,\mathbf{k}_a)|^2 =|\mathbf{e}\cdot\mathbf{F}_{\text{pw}a}(\mathbf{r}_0,\mathbf{k}_a)|^2+|\mathbf{e}\cdot\mathbf{F}_{\text{pws}}(\mathbf{r}_0,\mathbf{k}_s)|^2. \tag{54}$$

We can then write Eq. (53) by replacing the full radiation term by

$$\frac{3P_0(\omega_0)}{8\pi}\frac{n_a^3}{n^2(z_0)}\int_0^{\pi/2}\sin\theta_a d\theta_a\int_0^{2\pi}[|\mathbf{e}\cdot\mathbf{F}_{\text{pw}a}(\mathbf{r}_0,\mathbf{k}_a)|^2 + |\mathbf{e}\cdot\mathbf{F}_{\text{pws}}(\mathbf{r}_0,\mathbf{k}_s)|^2]d\phi. \tag{55}$$

Expression (55) shows that for the full radiation modes, the power is emitted through running waves in the air and in the substrate. Let us consider a detector located in the air and placed at the infinite from the dipole (Fig. 6). This detector receives the power $d^2P_d^a$, which is emitted in the infinitesimal solid angle $\sin\theta_a d\theta_a d\phi$. Such a power comes only from running waves in the air, so only the full radiative modes are concerned. From Eq. (55), one can express this power by

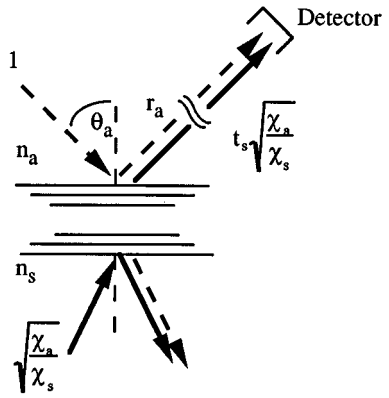


FIG. 6. Plane-wave fields $F_{\mathrm{pw}a}$ (solid lines) and $F_{\mathrm{pws}}$ (dashed lines) involved in the radiation pattern at the infinite.

$$\frac{d^2P_d{}^a}{P_0(\omega_0)} = \frac{3n_a{}^3}{8\pi n^2(z_0)} \{R_a|\mathbf{e}\cdot\mathbf{F}_{\mathrm{pw}a}(\mathbf{r}_0,\mathbf{k}_a)|^2 + T_s|\mathbf{e}\cdot\mathbf{F}_{\mathrm{pws}}(\mathbf{r}_0,\mathbf{k}_s)|^2 + (\mathrm{TM\ \ term})\} \times \sin\theta_a d\theta_a d\phi, \tag{56}$$

where $R_a = r_a r_a^*$ is the intensity reflection coefficient for a plane wave incoming on the stack from the air and $T_s = (\chi_a/\chi_s) t_s t_s^*$ is the intensity transmission coefficient for a plane wave incoming on the stack from the substrate. Equation (56) allows us to determine the radiation pattern in the air, normalized by the total power radiated by the dipole in free space.

Similarly, now consider the detector located in the substrate with $\theta_s < \theta_c$. The power $d^2P_d^s$, which is emitted by the dipole in the infinitesimal solid angle $\sin\theta_s d\theta_s d\phi$, is given by

$$\frac{d^2P_d{}^s}{P_0(\omega_0)} = \frac{3n_s{}^3}{8\pi n^2(z_0)} \{T_a|\mathbf{e}\cdot\mathbf{F}_{\mathrm{pw}a}(\mathbf{r}_0,\mathbf{k}_a)|^2 + R_s|\mathbf{e}\cdot\mathbf{F}_{\mathrm{pws}}(\mathbf{r}_0,\mathbf{k}_s)|^2 + (\mathrm{TM\ \ term})\} \times \sin\theta_s d\theta_s d\phi. \tag{57}$$

Let us now consider a guided mode in TE polarization. The guided power $d\mathbf{P}_g$, which is emitted in the infinitesimal angle $d\phi$, is given by

$$\frac{dP_g}{P_0(\omega_0)} = \frac{3}{8\pi} \frac{cN_{\mathrm{eff}}{}^2}{\omega_0 n^2(z_0)} |\mathbf{e}\cdot\mathbf{F}_g(\mathbf{r}_0,\mathbf{k}_g)|^2 d\phi. \tag{58}$$

To end our analysis, we may be interested in the spontaneous lifetime of the dipole, defined as $\tau = 1/\gamma$. It is simply given by

$$\frac{\tau}{\tau_0} = \frac{P_0(\omega_0)}{P}, \tag{59}$$

where $\tau$ and $\tau_0$ are the spontaneous emission lifetimes of the dipole in the stack and in free space, respectively.

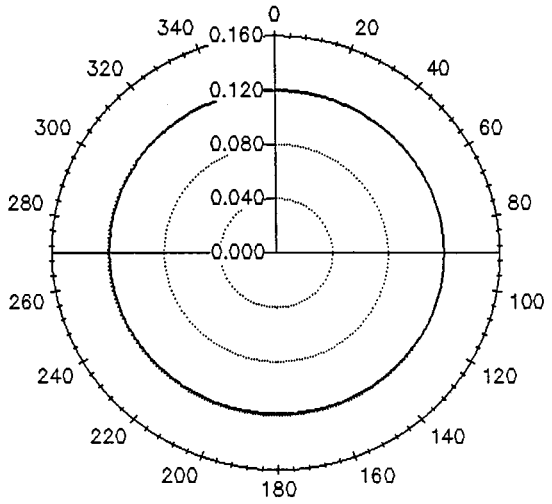


FIG. 7. Free space radiation pattern in a plane perpendicular to the dipole vector.

## VI. SPONTANEOUS EMISSION OF ERBIUM ATOMS PLACED INTO A MULTILAYER DIELECTRIC MICROCAVITY

This part of the paper shows a numerical example using the theory presented in the previous parts. It deals with the problem of the infrared ($\lambda_0 = 1.53\ \mu$m) radiation emitted by an erbium atom, where we assume that this atom can be represented by a dipole having its **e** vector along the $y$ axis. Let us first consider radiation in free space. Figure 7 shows the radiation pattern in the plane $xz$ (i.e., perpendicular to the dipole moment), which has been computed from Eq. (56). In this plane the isotropic emitted power is $d^2P_d^a = 0.12\, P_0(\omega_0) d\Omega$, where $d\Omega = \sin\theta d\theta d\phi$ stands for the infinitesimal solid angle. Integration of this radiation pattern in the whole space gives $P_0(\omega_0)$, as expected (see Eqs. 49 and 52).

Let us take now the same dipole, located at various positions into a multilayer microcavity. The microcavity considered here can be described by $HLHLHL\ 2H\ LHLHLH$, where $H$ and $L$ denote respectively high ($n_H = 2.181$) and low ($n_L = 1.477$) refractive index layers, whose optical thicknesses are $\lambda_0/4$. The structure is deposited on a substrate of refractive index $n_s = 1.444$. This design corresponds to a $\lambda/2$ microcavity with a quality factor $Q = \lambda_0/\Delta\lambda = 40$ (see Fig. 8),

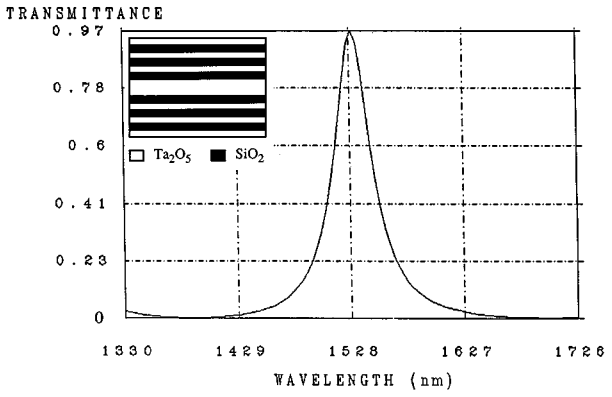


FIG. 8. Transmittance and microcavity design.

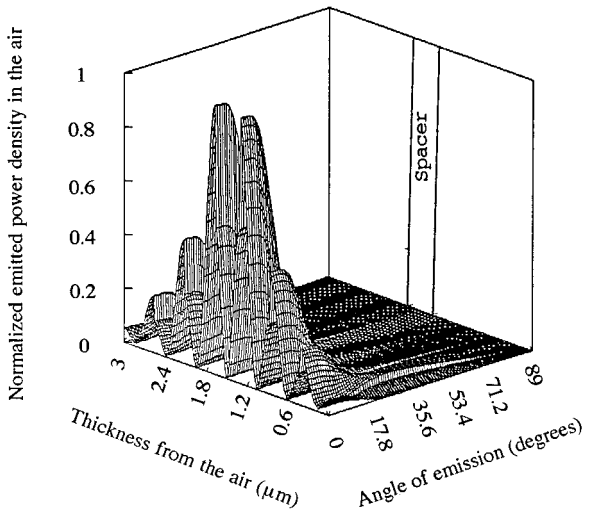


FIG. 9. Normalized emitted power in the air $(d^2P_d^a)/[P_0(\omega_0)d\Omega]$ for every direction and every location of the dipole in the stack.

and of total thickness 2.956 $\mu$m. We have chosen such refractive index figures because it corresponds to a microcavity made by the use of a plasma assisted deposition technique (ion plating), with, respectively, $Ta_2O_5$ and $SiO_2$ as high and low refractive index dielectric materials.

Consider the radiation pattern in the $xz$ plane for the dipole lying along the $y$ axis inside the cavity. Figure 9 shows the normalized power density $(d^2P_d^a)/[P_0(\omega_0)d\Omega]$ emitted in the air for every directions $\theta$ (in the range 0°–89°), and for every locations of the dipole in the stack. We can see, for example, that the power emitted in normal incidence (i.e., for $\theta$=0°) drastically depends on the location of the dipole in the stack [7]. For the computation, we use the microscopic electric field seen by the atom, given by the Clausius-Mossoti-Lorentz-Lorenz equation [34]

$$\mathbf{E}_{\text{micro}}=\frac{3n(z_0)^2}{2n(z_0)^2+1}\,\mathbf{E}_{\text{macro}}. \tag{60}$$

Let us define first the nonresonant case, where the dipole is located in the middle of this λ/2 cavity (i.e., at 1.478 $\mu$m—see Fig. 10). From Fig. 9 we see that the emission in normal incidence is completely inhibited. Figure 10 is a polar cut of Fig. 9 and shows the radiation pattern of such a dipole in the air and in the substrate. The emission in normal direction in the air is $d^2P_d^a=6\times10^{-3}\,P_0(\omega_0)d\Omega$ and is 20 times smaller than in free space (see Fig. 7). It is clear that this location, referred to as ''position 1,'' must be avoided in order to favor emission in normal incidence. Integration of this power in every directions and in the two polarizations gives the radiative power, which can exit the stack. One finds 0.03 $P_0(\omega_0)$.

We can now define the resonant case (referred to as ''position 2''), where the dipole is located on the interfaces between the spacer and the low refractive index layer (see Fig. 11). From Fig. 9 we know that the emission in normal incidence is enhanced. Figure 11 gives the radiation pattern of such a dipole in the air and in the substrate. The emission is well directed (10° around the normal) and is stronger in the substrate than in the air, this last point being due to the

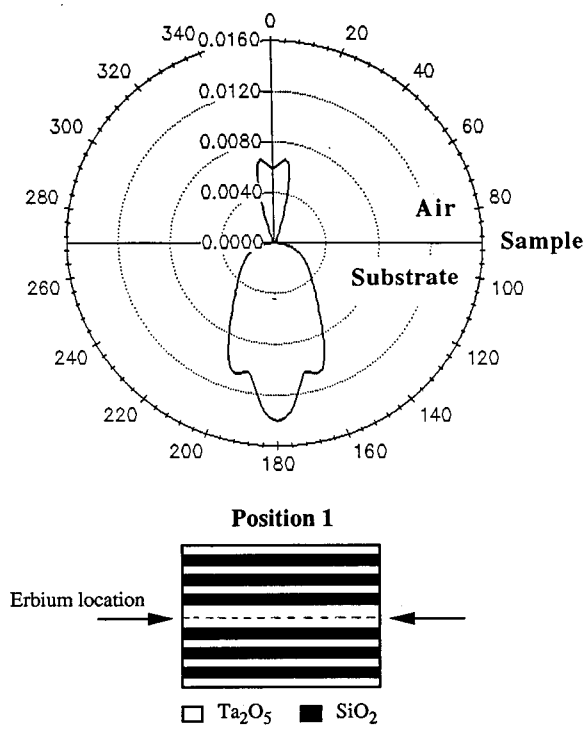


FIG. 10. Position 1: dipole location and radiation pattern.

dissymmetry of the microcavity. The emission in the normal direction in the air is $d^2P_d^a=0.8\,P_0(\omega_0)d\Omega$, and is 6.6 times higher than in free space (see Fig. 7). The total radiative power, which can exit the stack, is then 0.78 $P_0(\omega_0)$.

Consider now emission into the guided modes. Figure 12 gives the normalized emitted power $P_g/P_0$ in the various TE

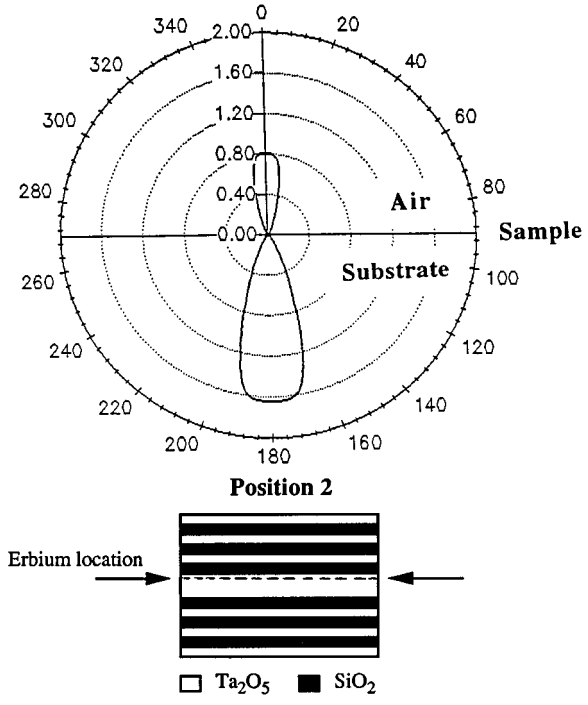


FIG. 11. Position 2: dipole location and radiation pattern.

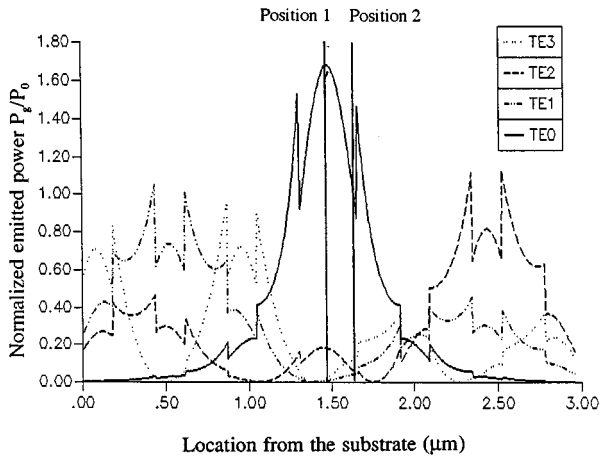


FIG. 12. Normalized emitted power $P_g/P_0$ in the various TE guided modes versus the dipole location.

guided modes [integration of Eq. (58) over $\phi$], versus the dipole location in the stack.

For the ''position 1'' dipole location (i.e., in the middle of the microcavity, see Fig. 10), the stronger emission is in the $TE_0$ mode, which is quite strong [1.67 $P_0(\omega_0)$] at this place. Figure 13 gives the emitted power in the various guided modes and in the radiative modes. Emission in the TE modes is stronger than in the TM ones because of the dipole orientation along the $y$ axis. Summation of these guided powers and of the radiative power gives the total power $P$ emitted by the dipole in this radiative nonresonant case. One finds $P=(1.95+0.03)\ P_0(\omega_0)=1.98\ P_0(\omega_0)$, and the normalized lifetime [see Eq. (59)] is therefore $[P_0(\omega_0)/P]=(1/1.98)\approx 0.5$.

This lifetime is two times shorter than in free space because the $TE_0$ mode is in this case a strong canal of relaxation for the dipole (see Fig. 13). Such a configuration achieves in fact a really good control of the spontaneous emission into the guided mode $TE_0$, and would therefore be of great interest for a guided wave device.

We consider now the ''position 2'' dipole location (i.e., at the interface of the spacer (see Fig. 11)). Figure 14 gives the power emitted in the various guided modes and in the radiative modes. In this case, the power is shared between the $TE_0$, $TM_0$, and $TE_3$ modes. The total power $P$ emitted by the dipole in the radiative and in the guided modes is $P=(1.39$

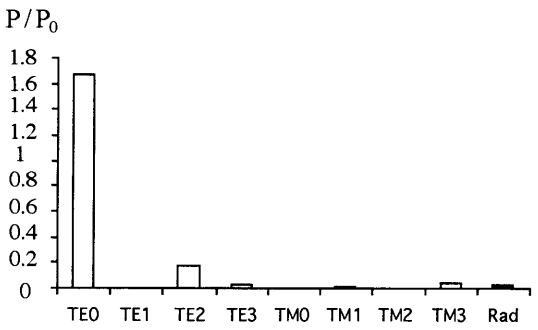


FIG. 13. Position 1: contribution of the guided and radiative powers.

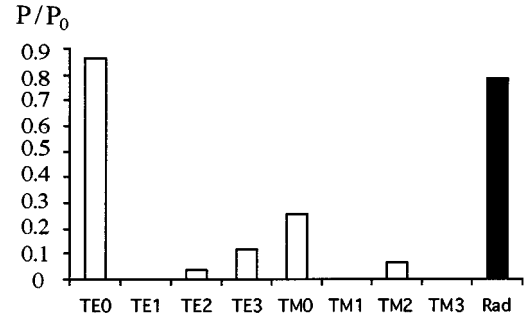


FIG. 14. Position 2: contribution of the guided and radiative powers.

$+0.78)\ P_0(\omega_0)=2.17\ P_0(\omega_0)$ and the normalized lifetime is 0.46, which is about the same as for the previous dipole location. Although this resonant case partly confines the radiation in normal incidence, the microcavity strongly suffers from emission in the guided modes.

## VII. CONCLUSION

We have presented a classical electromagnetic theory describing spontaneous emission in multilayer dielectric structures. This theory is based on a modal field expansion of the total electric field emitted by the dipole. In Secs. II and III we have presented a complete set of cavity modes, and how these modal fields (except the guided ones) can be derived from plane waves incoming on the stack from the air and from the substrate. Once the normalization of these modal fields has been achieved, we have extended our analysis to three dimensions, in order to treat the spontaneous emission of a dipole located in the stack, in terms of cavity modes. This approach gives the power emitted by the dipole in every direction in the air, in the substrate, and in the guided modes.

In Sec. VI, we have investigated numerically the radiative properties in the infrared ($\lambda_0=1.53\ \mu$m) of an erbium atom located at various positions in a particular dielectric microcavity. We have shown that the radiation pattern can be very different depending on the location of the dipole in the stack. Precisely, we have investigated two positions in the stack; one favors the emission in the guided modes and could be of great interest in building a guided wave device. The other one is known to favor the emission in the direction normal to the stack, and is usually implemented to build vertical emitting devices. In this last case, although the emission is well directed in a normal direction, the major part of the power is emitted into the guided modes. Although the radiation pattern is very different for the two locations of the dipole considered above, calculations show that its lifetime is about the same. In other words, if the dipole can not relax in the radiative modes that can exit the structure, it will strongly relax into the guided modes and vice versa. In conclusion the lifetime is not strongly affected. Nevertheless, the possibility of partially controlling spontaneous emission makes these planar structures of great interest for building high emissive devices such as directive light-emitting diodes or low threshold microlasers [32].

## ACKNOWLEDGMENTS

The authors are very grateful to C. Amra, S. Robert, F. Flory, and E. Pelletier for their efficient and helpful contributions. We also acknowledge stimulating and clarifying discussions with J. Y. Courtois, C. Fabre, J. M. Gérard, and V. Berger. The Direction des Recherches, Etudes et Techniques—French Ministry of Defense (DRET) and the Centre National de la Recherche Scientifique (CNRS) have sponsored this research. Numerical simulations have been performed on the CCSJ (Centre de Calcul de St Jérôme-Marseille), with financial support of the Région Provence-Alpes-Côte-d'Azur.


## APPENDIX A: DERIVATION OF EQS. (48) AND (54)

Using Eqs. (23a) and (23b) we can write

$$|\mathbf{e}\cdot\mathbf{F}_{fr-}(\mathbf{r}_0,\mathbf{k}_a)|^2=\tfrac{1}{2}|\mathbf{e}\cdot\mathbf{F}_{\mathrm{pw}a}(\mathbf{r}_0,\mathbf{k}_a)+\mathbf{e}\cdot\mathbf{F}_{\mathrm{pws}}(\mathbf{r}_0,\mathbf{k}_s)e^{i(\phi_{ra}-\phi_{ta}-\pi/2)}|^2=\tfrac{1}{2}\{|\mathbf{e}\cdot\mathbf{F}_{\mathrm{pw}a}(\mathbf{r}_0,\mathbf{k}_a)|^2+|\mathbf{e}\cdot\mathbf{F}_{\mathrm{pws}}(\mathbf{r}_0,\mathbf{k}_s)|^2$$
$$+\{[\mathbf{e}\cdot\mathbf{F}_{\mathrm{pw}a}(\mathbf{r}_0,\mathbf{k}_a)^*][\mathbf{e}\cdot\mathbf{F}_{\mathrm{pws}}(\mathbf{r}_0,\mathbf{k}_s)]e^{i(\phi_{ra}-\phi_{ta}-\pi/2)}+[\mathbf{e}\cdot\mathbf{F}_{\mathrm{pw}a}(\mathbf{r}_0,\mathbf{k}_a)][\mathbf{e}$$
$$\cdot\mathbf{F}_{\mathrm{pws}}(\mathbf{r}_0,\mathbf{k}_s)^*]e^{-i(\phi_{ra}-\phi_{ta}-\pi/2)}\}\} \tag{A1}$$

and

$$|\mathbf{e}\cdot\mathbf{F}_{fr+}(\mathbf{r}_0,\mathbf{k}_a)|^2=\tfrac{1}{2}|\mathbf{e}\cdot\mathbf{F}_{\mathrm{pw}a}(\mathbf{r}_0,\mathbf{k}_a)+\mathbf{e}\cdot\mathbf{F}_{\mathrm{pws}}(\mathbf{r}_0,\mathbf{k}_s)e^{i(\phi_{ra}-\phi_{ta}+\pi/2)}|^2=\tfrac{1}{2}\{|\mathbf{e}\cdot\mathbf{F}_{\mathrm{pw}a}(\mathbf{r}_0,\mathbf{k}_a)|^2+|\mathbf{e}\cdot\mathbf{F}_{\mathrm{pws}}(\mathbf{r}_0,\mathbf{k}_s)|^2$$
$$+\{[\mathbf{e}\cdot\mathbf{F}_{\mathrm{pw}a}(\mathbf{r}_0,\mathbf{k}_a)^*](\mathbf{e}\cdot\mathbf{F}_{\mathrm{pws}}(\mathbf{r}_0,\mathbf{k}_s)]e^{i(\phi_{ra}-\phi_{ta}+\pi/2)}$$
$$+[\mathbf{e}\cdot\mathbf{F}_{\mathrm{pw}a}(\mathbf{r}_0,\mathbf{k}_a)][\mathbf{e}\cdot\mathbf{F}_{\mathrm{pws}}(\mathbf{r}_0,\mathbf{k}_s)^*]e^{-i(\phi_{ra}-\phi_{ta}+\pi/2)}\}\} \tag{A2}$$

using the fact that $e^{i(\phi_{ra}-\phi_{ta}-\pi/2)}+e^{i(\phi_{ra}-\phi_{ta}+\pi/2)}=0$, we get

$$|\mathbf{e}\cdot\mathbf{F}_{fr-}(\mathbf{r}_0,\mathbf{k}_a)|^2+|\mathbf{e}\cdot\mathbf{F}_{fr+}(\mathbf{r}_0,\mathbf{k}_a)|^2=|\mathbf{e}\cdot\mathbf{F}_{\mathrm{pw}a}(\mathbf{r}_0,\mathbf{k}_a)|^2$$
$$+|\mathbf{e}\cdot\mathbf{F}_{\mathrm{pws}}(\mathbf{r}_0,\mathbf{k}_s)|^2. \tag{A3}$$

In an infinite and homogeneous medium, the fields $F_{\mathrm{pw}a}$ and $F_{\mathrm{pws}}$ become $\mathbf{u}(\mathbf{k}_a)$ and $\mathbf{u}(\mathbf{k}_s)$, respectively, with $\mathbf{k}_a=\beta x+\xi y+\chi z$, and $k_s=\beta x+\xi y-\chi z$. We can consider the $\mathbf{e}$ vector along the $y$ axis without loss of generality. Equation (A3) becomes

$$|\mathbf{e}\cdot\mathbf{F}_{fr-}(\mathbf{r}_0,\mathbf{k})|^2+|\mathbf{e}\cdot\mathbf{F}_{fr+}(\mathbf{r}_0,\mathbf{k})|^2=2|\mathbf{e}\cdot\mathbf{u}(\mathbf{k})|^2. \tag{A4}$$

## APPENDIX B: DERIVATION OF THE GUIDED MODE POWER

From Eqs. (41) and (46) it is clear that the guided mode contribution to the power emitted by the dipole is proportional to

$$\sum_{X_g}\int_{O_g}\delta_\Gamma(\omega_0-\omega_k)|\mathbf{e}\cdot\mathbf{F}_g(\mathbf{r}_0,\mathbf{k}_g)|^2 d\beta d\xi, \tag{B1}$$

where the integration is performed on the $O_g$ circle in the $k$ space (see Fig. 4).

Since $\omega_0-\omega_k\ll\omega_0$, we can consider that $\chi_g$ is not $\omega$- dependent. This implies that in polar coordinates

$$d\beta d\xi=k_g dk_g d\phi=\frac{\omega}{c^2}N_{\mathrm{eff}}^2 d\omega d\phi. \tag{B2}$$

$k_g=(\beta^2+\chi^2)^{1/2}$ is the modulus of the guided wave-vector $\mathbf{k}_g$, which stands in the $k_xk_y$ plane. $N_{\mathrm{eff}}=k_g/k_0$ is the effective refractive index of the considered guided mode. Taking as previously $\Gamma=0$, expression (B1) reads

$$\frac{\omega_0}{c^2}\sum_{k_g}N_{\mathrm{eff}}^2\int_0^{2\pi}|\mathbf{e}\cdot\mathbf{F}_g(\mathbf{r}_0,\mathbf{k}_g)|^2 d\phi. \tag{B3}$$


[1] E. M. Purcell, Phys. Rev. **69**, 681 (1946).
[2] D. Kleppner, Phys. Rev. Lett. **47**, 233 (1981).
[3] K. H. Drexhage, in *Progress in Optics*, edited by E. Wolf (North-Holland, Amsterdam, 1974), Vol. XII, p. 163.
[4] H. Kuhn, J. Chem. Phys. **53**, 101 (1970).
[5] K. H. Tews, J. Lumin. **9**, 223 (1974).
[6] C. Amra, J. Opt. Soc. Am. A **10**, 365 (1993).
[7] X.-P. Feng and K. Ujihara, Phys. Rev. A **41**, 2668 (1990).
[8] S. D. Brorson, H. Yokoyama, and E. P. Ippen, IEEE J. Quantum Electron. **26**, 1492 (1990).
[9] G. Bjork, S. Machida, Y. Yamamoto, and K. Igeta, Phys. Rev. A **44**, 669 (1991).
[10] S. T. Ho, S. L. McCall, and R. E. Slusher, Opt. Lett. **18**, 909 (1993).
[11] K. Kakazu and Y. S. Kim, Phys. Rev. A **50**, 1830 (1994).
[12] D. G. Deppe, C. Lei, C. C. Lin, and D. L. Huffaker, J. Mod. Opt. **41**, 325 (1994).
[13] N. Koide and K. Ujihara, Opt. Commun. **111**, 381 (1994).

[14] N. J. Hunt, E. F. Shubert, D. L. Sivco, A. Y. Cho, R. F. Kopf, R. A. Logan, and G. J. Zydzik, in *Confined Electrons and Photons, New Physics and Application*, edited by C. Weisbuch and E. Burstein NATO ASI Series 3 (Plenum, New York, 1995), p. 701.
[15] F. DeMartini, F. Cairo, P. Mataloni, and F. Verzegnassi, Phys. Rev. A **46**, 4220 (1992).
[16] J. Dalibard, J. Dupond-Roc, and C. Cohen-Tannoudji, J. Phys. (Paris) **43**, 1617 (1982).
[17] R. J. Glauber and M. Lewenstein, Phys. Rev. A **43**, 467 (1991).
[18] K. Tsutsumi, Y. Imada, H. Hirai, and Y. Yuba, IEEE J. Lightwave Technol. **6**, 590 (1988).
[19] H. A. Macleod, *Thin Film Optical Filters* (Hilger London, 1986), pp. 11–48.
[20] Y. Yamamoto, S. Machida, Y. Horikoshi, and K. Igeta, Opt. Commun. **50**, 337 (1991).
[21] D. Marcuse, *Light Transmission Optics* (Van Nostrand Reinhold, New York, 1972).
[22] D. Marcuse, *Theory of Dielectric Optical Waveguides*, 2nd ed. (Academic, New York, 1991).
[23] P. Benech, D. A. M. Khalil, and F. Saint André, Opt. Commun. **88**, 96 (1992).
[24] H. Kogelnik, *Guided-wave Optoelectronics*, edited by T. Tamir (Springer-Verlag, Berlin, 1988).
[25] P. Gerard, P. Benech, H. Ding, and R. Rimet, Opt. Commun. **108**, 235 (1994).
[26] J. J. Burke, J. Opt. Soc. Am. A **11**, 2481 (1994).
[27] P. Yeh, *Optical Waves in Layered Media* (Wiley, New York, 1988), p. 114.
[28] D. Marcuse, *Quantum Electronics* (Academic, New York, 1991), p. 19.
[29] J. Chilwell and I. Hodgkinson, J. Opt. Soc. Am. A **1**, 742 (1984).
[30] S. Haroche, in *Fundamental Systems in Quantum Optics* (North-Holland, Amsterdam 1991), p. 767.
[31] E. A. Hinds, in *Advanced in Atomic, Molecular and Optical Physics*, Suppl. 2 (Academic, New York, 1994).
[32] F. DeMartini, M. Marroco, P. Mataloni, L. Crescentini, and R. Loudon, Phys. Rev. A **43**, 2480 (1991).
[33] J. D. Jackson, *Classical Electrodynamics* (Wiley, New York, 1975).
[34] A. R. Von Hippel, *Dielectrics and Waves* (Wiley, New York, 1954).